RESEARCH

Biparametric MRI of the prostate radiomics model for prediction of pelvic lymph node metastasis in prostate cancers : a two-centre study

Chunxing Li[1,2†], Jisu Hu[3†], Zhiyuan Zhang[4], Chaogang Wei[1], Tong Chen[1], Ximing Wang[5], Yakang Dai[3] and Junkang Shen[1*]

Abstract

Objectives Exploring the value of adding correlation analysis (radiomic features (RFs) of pelvic metastatic lymph nodes and primary lesions) to screen RFs of primary lesions in the feature selection process of establishing prediction model.

Methods A total of 394 prostate cancer (PCa) patients (263 in the training group, 74 in the internal validation group and 57 in the external validation group) from two tertiary hospitals were included in the study. The cases with pelvic lymph node metastasis (PLNM) positive in the training group were diagnosed by biopsy or MRI with a short-axis diameter ≥ 1.5 cm, PLNM-negative cases in the training group and all cases in validation group were underwent both radical prostatectomy (RP) and extended pelvic lymph node dissection (ePLND). The RFs of PLNM-negative lesion and PLNM-positive tissues including primary lesions and their metastatic lymph nodes (MLNs) in the training group were extracted from T2WI and apparent diffusion coefficient (ADC) map to build the following two models by fivefold cross-validation: the lesion model, established according to the primary lesion RFs selected by t tests and absolute shrinkage and selection operator (LASSO); the lesion-correlation model, established according to the primary lesion RFs selected by Pearson correlation analysis (RFs of primary lesions and their MLNs, correlation coefficient > 0.9), t test and LASSO. Finally, we compared the performance of these two models in predicting PLNM.

Results The AUC and the DeLong test of AUC in the lesion model and lesion-correlation model were as follows: training groups (0.8053, 0.8466, $p = 0.0002$), internal validation group (0.7321, 0.8268, $p = 0.0429$), and external validation group (0.6445, 0.7874, $p = 0.0431$), respectively.

Conclusion The lesion-correlation model established by features of primary tumors correlated with MLNs has more advantages than the lesion model in predicting PLNM.

Keywords Magnetic resonance imaging, Radiomics, Prostate cancer, Pelvic metastatic lymph nodes

---

†Chunxing Li, Jisu Hu contributed equally to this work.

*Correspondence:
Junkang Shen
shenjunkang@suda.edu.cn
Full list of author information is available at the end of the article

Li *et al. BMC Medical Imaging*   (2024) 24:185

Page 2 of 10

Background

Cancer stands out as one of the fatal diseases people are facing all the time, hence prognosis or survival of cancer patients has become the focus of current research [1]. Studies have shown that pelvic lymph node metastasis (PLNM) in prostate cancer (PCa) patients is closely related to distant metastasis and biochemical recurrence after curative treatment and influence the prognosis and survival of patients [2, 3]. Therefore, it is particularly important to accurately identify the PLNM of localized PCa in patients [4].

To evaluate whether a PCa patient has PLNM, clinical workers initially developed various prediction models based on the clinical and biopsy information, such as the Briganti or MSKCC nomograms or Partin Tables [5–7]. With the emergence of prostate magnetic resonance imaging (MRI) [8, 9], predictive factors based on MRI information have been favoured by researchers, such as the MRI-based qualitative characteristics of primary PCa lesions (measured tumour size, extraprostatic extension and seminal vesicle invasion) [10, 11]. MRI-targeted biopsies have been used as a substitute for systematic biopsy to obtain a more accurate Gleason score [12], and the MRI-based quantitative RFs and deep features of the primary lesions are extracted by radiomics and deep learning methods [13]. Current research is focused on mining primary lesion features that are conducive to predicting PLNM and on improving the performance of using primary lesion features in predicting PLNM. It is not known whether the RFs of pelvic metastatic lymph nodes (MLNs) can help improve the performance of the radiomics model of primary lesions in predicting PLNM in PCa.

Currently, extended pelvic lymph node dissection(ePLND) is the gold standard for the diagnosis of PLNM in PCa. According to this standard, imaging findings of pelvic LNs with an oval short axis diameter of ≥1 cm or a round short axis diameter of ≥0.8 cm are considered to indicate malignant LNs [10, 14–16]. Using this short axis diameter criteria, studies have shown that the pooled sensitivity of conventional MRI is 39% and the pooled specificity is 82% [17], and the pooled sensitivity of diffusion-weighted imaging (DWI) is 41% and the pooled specificity is 94% [18]. MRI evaluation of PLNM has low sensitivity and high specificity. A meta-analysis has previously shown that with improvement of the diagnostic criteria, that is, the increase in the positive lymph node threshold, there is an increase in the specificity of MRI diagnosis of MLNs. When the threshold is greater than or equal to 1.5 cm, the specificity is very high (up to 98 − 100%) [19]. Therefore, for patients with biopsy-confirmed PCa, when biparametric MRI (bpMRI) comprising T2-weighted imaging (T2WI) and DWI showed that the LNs (short axis diameter ≥1.5 cm) were round or oval

or that the hilum of the lymph node had disappeared, or obviously high signal on high b-value DWI, the author had reason to believe that the abnormal LNs were MLNs.

Cancer lesions of pelvic LNs are metastatic from primary lesions, and thus, metastatic tissue in pelvic LNs should have the metastatic characteristics of the primary lesions. Their RFs should be closely related to those representing the metastatic characteristics of the primary lesions. With the help of the RFs of pelvic MLNs, it would be an interesting research direction to screen for more reasonable RFs of primary lesions and thus build a better predictive model. Here, we conducted this study to extract the RFs of pelvic metastatic LNs and primary lesions respectively, and performed correlation analysis to obtain RFs of primary tumors correlated with metastatic lymph nodes. Finally, we established an radiomics model to check its performance in predicting PLNM.

Patients and methods

Patients

A total of 394 PCa patients from two tertiary care centers, Center 1 and Center 2, were included in the study. Patients from Center 1 were enrolled between May 2016 and July 2021, while those from Center 2 were enrolled between January 2019 and May 2020. The training group, which consisted of 93 PLNM-positive and 170 PLNM-negative PCa patients, and the internal validation group, which included 19 PLNM-positive and 55 PLNM-negative PCa patients, were both from Center (1) The external validation group, comprising 14 PLNM-positive and 43 PLNM-negative PCa patients, was from Center (2) This retrospective study was approved by the institutional ethics committees of the two tertiary care centers. The requirement for informed patient consent was waived.

Inclusion of positive cases in the training group

All PCa patients enrolled in the training group were diagnosed as PLNM-positive by bpMRI. Drawing on previous studies that utilized MRI or CT to detect suspected pelvic LNs ≥1.5 cm, which were subsequently confirmed as MLNs after surgery [20–23], the present study also validated the diagnoses of 11 PLNM-positive patients in the training group. These included 4 patients diagnosed by biopsy and 7 diagnosed through pre- and post-treatment comparisons by MRI. For suspicious LNs diagnosed by bpMRI and with a short axis diameter ≥1.5 cm, the biopsy results and the decreased sizes of lymph nodes pre- and post-treatment were considered confirmation of metastasis. Therefore, we stipulated that metastatic LNs met the following requirements: (i) lymph nodes were round or oval, the hilum of the lymph node had disappeared or there was a heterogeneous signal intensity on high-resolution T2WI; (ii) high b-value DWI showed obvious high signal intensity, and apparent diffusion
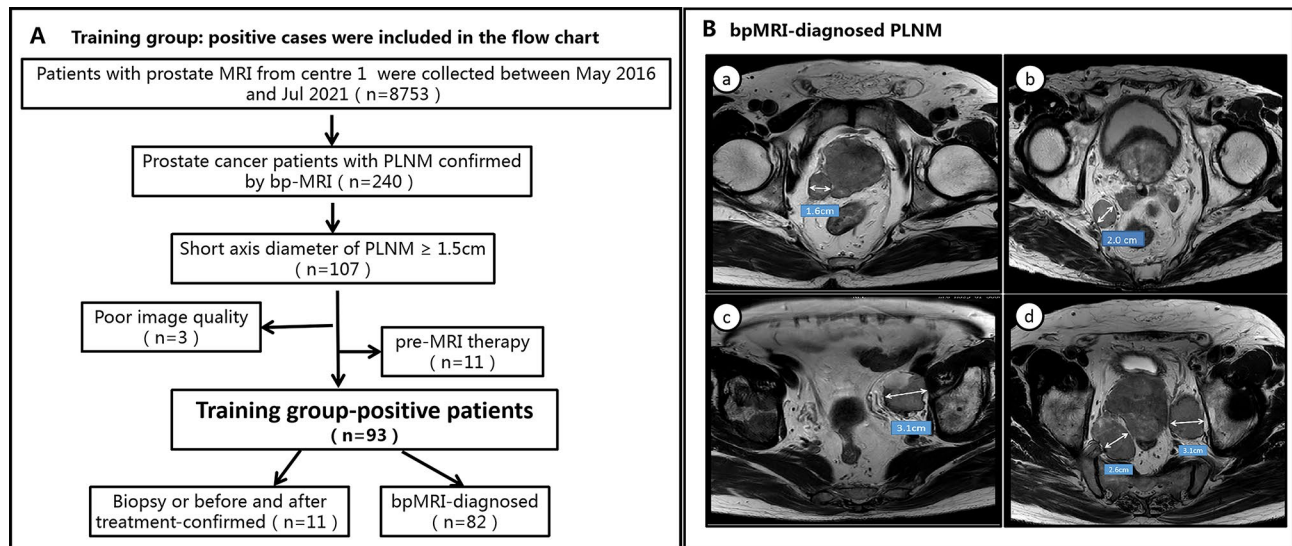
Fig. 1 **A** shows the inclusion and exclusion criteria of positive patients in the training group. **B** shows bpMRI-diagnosed PLNM: four patients (a, b, c, d) with PLNM shown on T2WI (DWI was not added due to length) were included according to the criteria of pelvic metastasis LNs specified herein; a-d representative images showed that abnormal LNs with enlarged morphology (short axis diameter > 1.5 cm) and heterogeneous signals could be seen in the right paraprostatic area, the mesorectum, left iliac vessels and bilateral iliac vessels, respectively. RP: radical prostatectomy; PLNM = pelvic lymph node metastasis; bpMRI = biparametric MRI (T2WI and DWI)
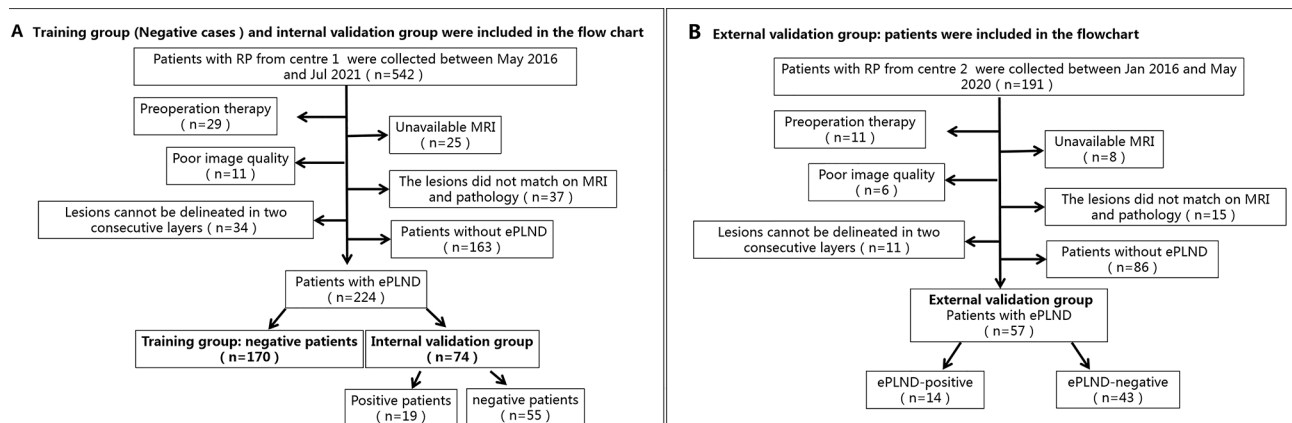

Fig. 2 **A** shows the inclusion and exclusion criteria of the training group (negative cases) and the internal validation group. **B** shows the inclusion and exclusion criteria of the external validation group. ePLND = extended pelvic lymph node dissection

coefficient (ADC) map showed obvious low signal intensity; and (iii)the diameter of the short axis of abnormal LNs diagnosed by bpMRI was ≥1.5 cm. A flow diagram of the patient selection process with the inclusion and exclusion criteria is provided in Fig. 1(A, B).

Inclusion criteria of the training group (negative cases) and validation groups

The inclusion criteria of the training group (negative cases) and validation groups were patients who underwent both RP and ePLND. None of the patients had a history of previous surgery, radiotherapy or adjuvant therapies for PCa before their prostate MRI. The inclusion/exclusion criteria are shown in detail in Fig. 2 (A, B).

MRI protocols and sequence selection

All patients underwent 3.0T multiparametric MRI(mpMRI)or bpMRI scans with a pelvic phased-array coil, and the scan protocols and sequence were in accordance with Prostate Imaging Reporting and Data System version 2.0 or 2.1 (including T2WI, DWI, and/or dynamic contrast-enhanced (DCE) imaging). ADC maps were calculated on a designated workstation with b values of 100 and 1000 s/mm2. The manufacturers and models of the MR machines in the two hospitals are as follows: at centre 1, Philips Ingenia, Best, Netherlands; and at centre 2: Siemens, skyra, Erlangen, Germany.

Since recent studies have shown that bpMRI may serve as a faster, cheaper, gadolinium-free alternative to mpMR [24]. Therefore, in this study we selected bpMRI as the

research sequence. Additionally, a study has previously shown that compared with high b-value DWI, using an ADC map for RFs extraction could provide superior stability [25]. Finally, we selected high-resolution T2WI and ADC maps for RFs extraction. The scan parameters and machine models of the hospitals are listed in Supplementary 1.

Reference standard for pathology

All patients underwent a TRUS-guided 12-core systematic biopsy within 1 week after the prostate MRI scans. RP with ePLND was performed within 4 weeks after the prostate MRI scans. According to the ISUP 2005 and 2014 recommendations [26, 27], the histopathology of the specimens was assessed by experienced pathologists at the two hospitals.

In the evaluation of ePLNDs, the numbers and locations of normal LNs and MLNs were determined. According to the EAU risk group [28], RP with ePLND was performed in moderate-risk (unfavourable prognoses) and high-risk patients. Local LN dissection included dissection of the external iliac and obturator LNs. Expanded LN dissection included dissection of the obturator, external iliac, internal iliac, presacral and common iliac LNs. Four cases of biopsy-confirmed pelvic MLNs in the training group were found in the external iliac LN group in this study.

Segmentation of cancer lesions on T2WI and ADC maps

The T2WIs (DICOM format) of all enrolled patients were imported into ITK Snap software (v3.8; http://www.itksnap.org/pmwiki/pmwiki.php). The ROIs of the primary lesions and their metastatic LNs were manually delineated by slicing along the contour of the cancer lesion and avoiding any calcification, bleeding, cysts and other structures present in the primary lesion and MLNs. The volume of interest (VOI-1) of the primary lesion and VOI-2 of MLNs were finally obtained by multilayer fusion in ITK Snap. The ADC images were registered and resampled to the corresponding T2W images, and the annotations of the ADC images were copied from those of the T2W images.

Radiomic feature extraction, selection and construction

The RFs of PLNM-negative lesion and PLNM-positive including primary lesions and their MLNs in the training group were extracted using PyRadiomics (version 2.1.0; https://pyradiomics.readthedocs.io/en/2.1.0/), On this basis, this study refers to a new machine learning-based user-friendly software platform for automatic RFs extraction, feature selection, model building, model training and analysis [29] (Fig. 3). This study conducted a self-assessment of our work using the CLEAR checklist [30] and METRICS [31], which were submitted as Supplementary 2 and Supplementary 3.

We extracted features from the original images of the lesion area and metastatic LN area and from the images that were transformed by log (Sigma: [0.5,1,1.5]), logarithm, square, square root, exponential, gradient, lbp3d and wavelet (start_level: 1, level: 1, wavelet: Haar). Seven types of RFs were derived from the T2WI and ADC maps: first order, shape, gray level co-occurrence matrix (GLCM), gray level run length matrix (GLRLM), gray level size zone matrix (GLSZM), neighbourhood gray tone difference matrix (NGTDM), and gray level dependence matrix (GLDM). The following settings for feature
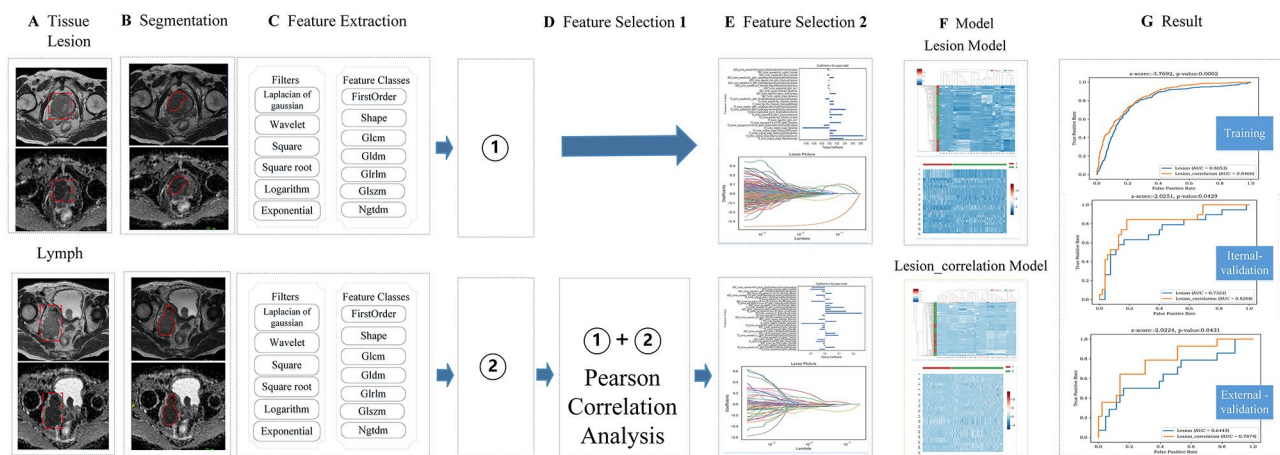

Fig. 3 shows the radiomics workflow in this study. **A** and **B** show the primary lesion and its metastatic pelvic LNs and the ROI on T2WI and ADC map. **C** shows the types of extraction of RFs of the primary lesion and its pelvic MLNs, respectively. **D** shows two pathways: ① shows that the extracted primary lesion features have no feature selection in the D link. ② shows that the extracted RFs of the primary lesion and its MLNs were performed by a Pearson correlation analysis for feature selection, and the primary lesion RFs were selected by Pearson correlation analysis. E shows that two pathways were performed by the LASSO algorithm for feature selection. F shows the establishment of the Lesion model and Lesion-correlation model. G shows the performance comparison of the two models in the training group and the internal and external validation groups. LASSO = absolute shrinkage and selection operator

Li *et al. BMC Medical Imaging*   (2024) 24:185

Page 5 of 10

extraction were used: b-spline interpolator, resampled pixel spacing of [1], pad distance of 10, bin width of 25, yoxel array shift of 300 and normalize scale of 100.

Prior to the feature selection, all RFs were normalized to zero mean and unit variance by standardization to prevent features with a large numerical range from dominating features with a small numerical range. Using the Pearson correlation analysis algorithm, the t test and lesast absolute shrinkage and selection operator (LASSO) algorithm were applied to screen for the best RFs for predicting PLNM status. The inter- and intraclass correlation coefficients (ICCs) between the extracted features of radiologists A (first time) and B were 0.7513–0.9799, and those of radiologist A (twice) were 0.7544–0.9748, which showed that the two signatures had good consistency. The Synthetic Minority Over-sampling Technique (SMOTE) was used to augment the RFs in the minority group of the training set [32].

The support vector machine (SVM) classifier was used to establish the radiomics model. When training the model, fivefold cross-validation was adopted and repeated 5 times to select the best training parameters and build the following two models: the lesion model, established according to the RFs selected directly by the t test and LASSO algorithm after extracting the primary lesion features; and the lesion-correlation model, established by first performing Pearson correlation analysis (correlation coefficient > 0.9) between the primary lesion features and MLN features, retaining only some of the primary lesion features that were closely correlated with MLN features, and second performing the t test and LASSO algorithm.

Statistical analysis
Patient age, PSA, pathological information and MRI stage were statistically analyzed by Statistical Package for Social Science (SPSS, version 21.0, https://www.ibm.com/cn-zh/ analytics/spss-statistics-software). A two-sample t test was used to compare the differences in age and PSA level, while chi-square or Fisher exact tests, as appropriate, were used to compare the differences in categorical variables (MRI-based stage, pathological information). Intra- and interclass correlation coefficients (ICCs) were assessed using the kappa test. The performance of the lesion model and lesion-correlation model was assessed with receiver operating characteristic (ROC) curves in the training group and internal and external validation groups. The area under the curve (AUC), accuracy, sensitivity and specificity were calculated. The differences in the AUC values of the two models were assessed by the DeLong test. There was a significant difference in the bilateral test ($P < 0.05$).

Results

Clinical characteristics
A total of 394 PCa patients were ultimately enrolled in our study. The patients with PLNM accounted for 93/263 (35.4%), 19/74 (26.7%) and 14/57 (24.6%) in the training, internal validation and external validation groups, respectively. In the training group, 93 positive patients had 163 metastatic LNs (bpMRI-diagnosed and short axis diameter ≥ 1.5 cm), and the average diameter of the metastatic LNs was 2.3 cm. The statistical results for the clinical, pathological and MRI data of each group are described in detail in the list (Table 1).

Feature extraction and model construction
To ensure the stability of the features, two radiologists independently delineated the ROIs slice by slice on the MR images of 30 patients.

Two groups of features (3748 features each) were extracted from VOI-1 and VOI-2. For the lesion model, the primary lesion RFs were screened by the t test and LASSO algorithm, and 27 features were ultimately selected, thereby establishing the lesion model. Additionally, ''T2_tumor_original_shape_Maximum2ddiametercolumn" had the highest weight coefficient and was positively correlated among all the features included in the lesion model (Fig. 4A). For the lesion-correlation model, the extracted features of the metastatic LNs and primary lesions were analyzed by Pearson correlation analysis algorithm, 280 features of the primary lesions were obtained, and then feature screening by the t test and LASSO algorithm was performed. Finally, 32 features were selected, thereby establishing the lesion-correlation model. Further, "T2_tumor_wavelet_LLL_glszm_ZoneEntropy" accounted for the highest weight coefficient and was positively correlated among all the features included in the lesion-correlation model (Fig. 4B).

Model comparison and validation
Table 2 shows the AUC and 95% CI of the lesion model and lesion-correlation model in the training group [0.8053 (95% CI: 0.7876–0.8230); 0.8466 (95% CI: 0.8317–0.8615)], internal validation group [0.7321 (95% CI: 0.5854–0.8787);0.8268 (95% CI:0.7096–0.9440)], and external validation group [0.6445 (95% CI:0.4618–0.8273); 0.7874 (95% CI:0.6466–0.9281)], respectively; The DeLong test of the AUC values of the lesion model and lesion-correlation model in the training and two validation groups were 0.0002, 0.0429 and 0.0431, respectively. The ROC curve, AUC, accuracy, sensitivity, specificity and DeLong test of the two models in the training, internal validation and external validation groups are shown in the following chart (Table 2 ; Fig. 5).

Table 1 The characteristics of the patients in the training and validation groups

Characteristic	Training group			Internal-validation group			External-validation group		
	PLNM (+)	PLNM (-)	*p*	PLNM (+)	PLNM (-)	*p*	PLNM (+)	PLNM (-)	*p*
	n=93	*n*=170		*n*=19	*n*=55		*n*=14	*n*=43	
age, mean	73.7204	70.8235	0.002*	71.25	69.7234	0.373	66.5455	68.625	0.412
PSA(ng/mL), mean	95.6	33.4	0.000*	63.4	35.7	0.000*	70.6	32.3	0.000*
MRI-based stage, No. (%)			0.000*			0.000*			0.000*
T2	2/93 (2.1)	130/170 (76.5)		3/19 (15.8)	29/55 (52.7)		5/14(35.7)	25/43(58.1)	
T3a	11/93 (11.8)	26/170 (15.3)		5/19 (26.3)	18/55 (32.7)		5/14(35.7)	11/43(25.6)	
T3b	36/93 (38.7)	14/170 (8.2)		11/19 (57.9)	8/55 (14.5)		4/14(28.6)	7/43(16.3)	
T4	44/93 (47.4)	0/170		0/19	0/55		0/14	0/43	
Bone metastasis, No. (%)	55/93 (59.1)								
MLN short-axis mean(cm)	2.3								
LNM number	164								
Biopsy findings, No. (%)			0.043*			0.000*			0.000*
GS 3+3	0	7/170 (4.1)		0/19	3/55 (5.5)		0/14	0/43	
GS 3+4	13/93 (14.0)	21/170 (12.4)		2/19 (10.5)	15/55 (27.3)		0/14	11/43 (25.6)	
GS 4+3	29/93 (31.2)	71/170 (41.8)		1/19 (5)	16/55 (29.1)		1/14 (7.1)	20/43 (46.5)	
GS≥4+4	51/93 (54.8)	71/170 (41.8)		16/19 (84.2)	21/55 (38.2)		13/14 (93.9)	12/43 (27.8)	
Surgical findings, No. (%)						0.000*			0.000*
GS 3+3	Non	10/170 (5.8)		0/19	4/55 (7.3)		0/14	0/43	
GS 3+4	Non	22/170 (12.9)		2/19 (10.5)	14/55 (25.5)		0/14	11/43 (25.6)	
GS 4+3	Non	67/170 (39.4)		1/19 (5)	16/55 (29)		1/14 (7.1)	21/43 (48.8)	
GS≥4+4	Non	71/170 (41.9)		16/19 (84.2)	21/55 (8.2)		13/14 (93.9)	11/43 (25.6)	
Pathological stage, No. (%)						0.000*			0.000*
T2	Non	135/170 (79.4)		4/19(21.1)	29/55 (52.7)		6/14 (42.8)	23/43 (53.5)	
T3a	Non	21/170 (12.3)		2/19(10.5)	18/55 (32.7)		4/14 (28.6)	13/43 (30.2)	
T3b	Non	14/170 (8.2)		10/19 (52.7)	8/55 (14.5)		4/14 (28.6)	7/43 (16.3)	
T4	Non	0/170		3/19 (15.8)	0/42		0/14	0/43	

PLNM=pelvic lymph node metastasis; MLN=metastatic lymph node; PSA=prostate-specific antigen

*P value<0.05

Discussion

LN metastatic lesions "flow" from primary lesions along lymphatic vessels and grow in the LNs. Although the growth environment differs from that of the primary lesions, the histological characteristics are the same, as demonstrated by the immunohistochemical examination results. Therefore, MLNs contain the cancer tissue derived from the primary lesions, which is more likely to reflect the metastatic characteristics of the primary lesions. Radiomics is an emerging research technology that reflects changes at the tumour tissue, cell and gene levels by mining the RFs of tumours [33, 34]. That is, the RFs of MLNs can reflect the metastatic characteristics of primary lesions. Therefore, it can be considered that a correlation analysis between the RFs of primary lesions and MLNs can better select the RFs of primary lesions reflecting metastatic characteristics. Unlike previous approaches focusing on the task of algorithm selection [11, 13, 35–37], in this study, the RFs of pelvic MLNs in PCa were extracted for the first time and used to effectively screen the RFs reflecting PLNM in primary lesions by the correlation analysis algorithm, optimizing the feature selection of the primary lesions. This study

results indicated that the lesion-correlation model had some advantages over the lesion model in predicting PLNM, the DeLong test of their AUC values in the training and two validation groups were 0.0002, 0.0429 and 0.0431,respectively, and confirmed that the RFs of primary lesions that were more predictive of PLNM could be screened by correlation analysis with the RFs of metastatic LNs.

The problem of locating and delineating metastatic lymph nodes on MR images must be solved before using the RFs of pelvic MLNs and primary lesions for correlation analysis. For MLNs confirmed by PLND, a previous study reported that only 30% of PLNMs were identified by CT or MRI, because most MLNs were less than 8 mm [17, 38], and 83% of them were ≤5 mm and 50% were ≤3 mm [39]. Relevant literature has also confirmed that the volume of MLNs in PLND is generally small, and most of them are not detectable on conventional MRI [40, 41], which makes it difficult to locate and delineate MLNs on the images. To solve the difficulty, this study stipulated specific inclusion criteria for the PLNM-positive patients in the training group, i.e., LNs with
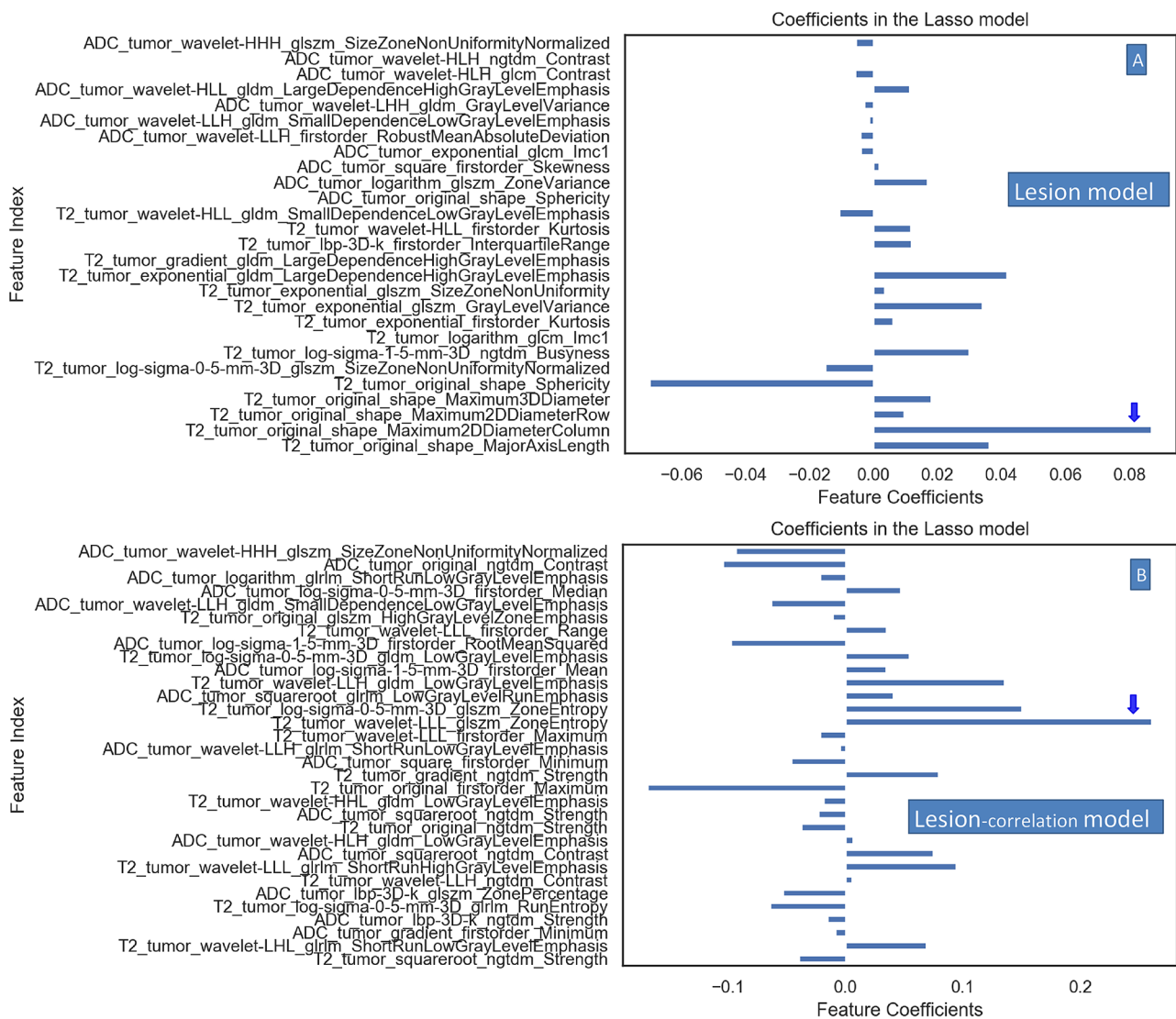
Fig. 4 (**A**, **B**) shows the radiomic features and weights of the feature coefficients in the lesion model and lesion-correlation model, respectively. Figure 4 (**A**, **B**) shows that in the feature coefficient column, the right side indicates a positive correlation, and the left side indicates a negative correlation. The feature weights were generated by the lasso algorithm. Figure 3-A shows that among all the features (n = 27), "T2_tumor_original_shape_Maximum2d-diameter column" accounted for the highest weight coefficient and was positively correlated (blue arrow) in the Lesion model. Figure 3-B shows that among all the features (n = 32), "T2_tumor_wavelet_ LLL_glszm_ZoneEntropy" accounted for the highest weight coefficient and was positively correlated in the Lesion-correlation model (blue arrow). LASSO = absolute shrinkage and selection operator

Table 2 The performance of the two models in the primary training and validation groups

	Models	AUC	95%CI	Accuracy	Sensitivity	Specificity	Delong-test p-value
Training group	Lesion radiomics	0.8053	[0.7876-0.8230]	0.7635	0.714	0.7906	0.0002
	Lesion-correlation radiomics	0.8466	[0.8317-0.8615]	0.7511	0.8344	0.7053	
Internal validation group	Lesion-radiomics	0.7321	[0.5854-0.8787]	0.6622	0.6842	0.6545	0.0429
	Lesion-correlation radiomics	0.8268	[0.7096-0.9440]	0.7838	0.8421	0.7636	
External validation group	Lesion-radiomics	0.6445	[0.4618-0.8273]	0.6491	0.5	0.6977	0.0431
	Lesion-correlation radiomics	0.7874	[0.6466-0.9281]	0.807	0.6429	0.8605	

AUC = area under the receiver operating curve; CI = confidence interval
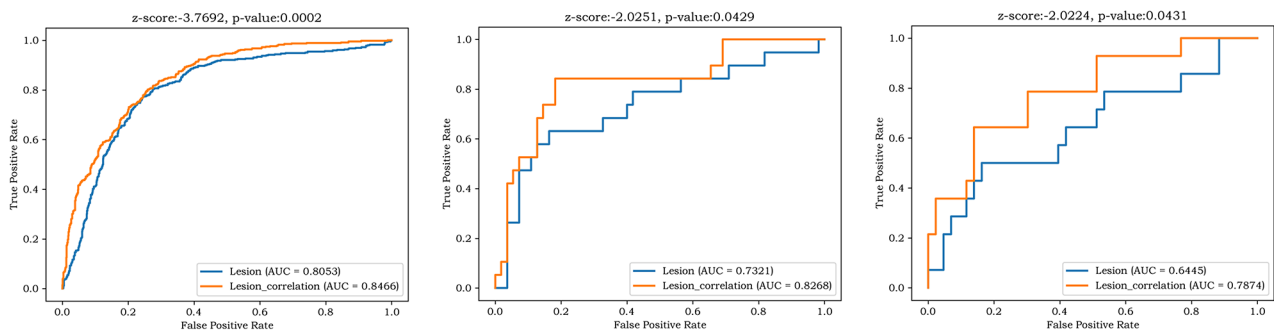
Fig. 5 shows that the ROC curves, AUC and DeLong test of AUC in the lesion model and lesion-correlation model were 0.8053, 0.8466, and 0.0002 in the training groups, 0.7321, 0.8268, and 0.0429 in the internal validation group, and 0.6445, 0.7874, and 0.0431 in the external validation group, respectively. AUC = area under the receiver operating curve

abnormal signal intensity on bpMRI and those ≥ 1.5 cm in the short-axis diameter.

The premise of tumour metastasis is the aggressiveness of tumour cells and infiltrative growth in the surrounding stroma. The former reflects the attack of tumour cells on the surrounding tissues, such as the destruction of lymphatic vessels and blood vessels; and the latter reflects the growth of tumour cells in the surrounding tissues, resulting in local spread of the tumour. Regarding tumour aggressiveness, some studies have found that the homogeneity and entropy features from GLCM and GLRLM are significantly correlated with PCa aggressiveness and significantly differ between low- and intermediate/high-aggressive PCa, as defined by histopathology [42–44]. Our findings similarly showed that "T2_tumor_wavelet_ LLL_glszm_ zone Entropy" had the highest weight coefficient among all the features included in the correlation model; however, in contrast with previous studies, our entropy feature was extracted from GLSZM. The main reason may be that most of our data are from patients with highly aggressive PCa, and all of them have PLNM, which is partially consistent with previous studies involving the prediction of tumour PLNM [13, 45]. These findings indicated that the entropy feature of GLSZM from T2WI could be used as an important marker to predict PLNM in PCa. Among all the features included in the lesion model, this study found that "T2_tumor_original_ shape_ Maximum2d diameter column" had the highest weight coefficient, which described the regional feature of the internal tumour shape, and it also might reflect another feature of tumour metastasis, namely tumour infiltration, which mainly relates to the local spread of the tumour. Additionally, this study found that in both models, the weight coefficient of features ranked ahead were from T2WI, not from the ADC map (Fig. 4). We speculated that compared with the texture features from the ADC map, those from T2WI can better reflect the aggressiveness of tumors. In summary, these results indicated that the texture features obtained by correlation

analysis with MLNs might be of greater value in predicting LNM and worthy of further exploration.

Our study had several limitations. First, the majority of pelvic MLNs in the training group were diagnosed by prostate MRI, a minority of which were confirmed by biopsy or therapy. Second, deep features of pelvic MLNs were not extracted, and a deep learning algorithm will be applied in future research. Third, the cases in this paper underwent imaging with two types of imaging devices (Siemens and Philips), which were inconsistent in manufacturer performance and scanning parameters.

Conclusion

Radiomics allows for the extraction of a large number of RFs from VOIs. The selection of effective features will directly affect the performance of the prediction model. The correlation analysis algorithm with pelvic MLNs could be used to effectively screen the RFs of primary lesions that reflected the characteristics of PLNM, and improve the performance of the primary lesions in predicting PLNM and provide new insights into the feature selection process.

Abbreviations

PCa	Prostate cancer
RF	Radiomic feature
PLNM	Pelvic lymph node metastasis
MLN	Metastasis lymph node
mpMRI	Multiparametric MRI
bpMRI	Biparametric MRI
RP	Radical prostatectomy
LASSO	Absolute shrinkage and selection operator
ePLND	Extended pelvic lymph node dissection
T2WI	T2-weighted imaging
DWI	Diffusion-weighted imaging
DCE	Dynamic contrast-enhanced
ADC	Apparent diffusion coefficient
VOI	Volume of interest
ROC	Receiver operating characteristic
AUC	Area under the curve

Li *et al. BMC Medical Imaging*   (2024) 24:185

Page 9 of 10

Supplementary Information

The online version contains supplementary material available at https://doi.org/10.1186/s12880-024-01372-8.

Supplementary Material 1

Supplementary Material 2

Supplementary Material 3

Supplementary Material 4

Supplementary Material 5

Declarations

Ethics approval and consent to participate
The institutional ethics committee of two hospitals(The Second Affiliated Hospital of Soochow University, The First Affiliated Hospital of Soochow University) approved this study and waived the need for informed consent from patients.

Consent for publication
Not applicable.

Conflict of interest
The authors have no conflicts of interest to declare.

Author details
[1]Department of Radiology, The Second Affiliated Hospital of Soochow University, Suzhou, China
[2]Department of MRI Room, Yancheng First Hospital Affiliated Hospital of NanJing University Medical School, Yancheng, China
[3]Suzhou Institute of Biomedical Engineering and Technology, Chinese Academy of Sciences, Suzhou, China
[4]School of Medical Imaging, Biomedical Engineering, Xuzhou Medical University, Xuzhou, China
[5]Department of Radiology, The First Affiliated Hospital of Soochow University, Suzhou, China

References
1. Soltani M, Bonakdar A, Shakourifar N, Babaei R, Raahemifar K. Efficacy of location-based features for survival prediction of patients with glioblastoma depending on resection status. Front Oncol. 2021;11:661123.
2. Wilczak W, Wittmer C, Clauditz T, Minner S, Steurer S, Buscheck F, et al. Marked prognostic impact of minimal lymphatic tumor spread in prostate cancer. Eur Urol. 2018;74(3):376–86.
3. von Bodman C, Godoy G, Chade DC, Cronin A, Tafe LJ, Fine SW, et al. Predictingbiochemical recurrence-free survival for patients with positive pelvic lymphnodes at radical prostatectomy. J Urol. 2010;184(1):143–8.
4. Mottet N, Bellmunt J, Bolla M, Briers E, Cumberbatch MG, De Santis M, et al. EAU-ESTRO-SIOG guidelines on prostate cancer. Part 1: screening, diagnosis, and localtreatment with curative intent. Eur Urol. 2017;71(4):618–29.
5. Briganti A, Larcher A, Abdollah F, Capitanio U, Gallina A, Suardi N, et al. Updated nomogram predicting lymph node invasion in patients with prostate cancer undergoing extended pelvic lymph node dissection: the essential importance of percentage of positive cores. Eur Urol. 2012;61(3):480–7.
6. Memorial Sloan Kettering Cancer Center. Dynamic prostate cancer nomogram:coefficients. cited; https://www.mskccorg/nomograms/prostate/pre-op/coefficients. Last Updated: 2020;January 14.
7. Tosoian JJ, Chappidi M, Feng Z, Humphreys EB, Han M, Pavlovich CP, et al. Prediction of pathological stage based on clinical stage, serum prostate-specific antigen,and biopsy gleason score: partin tables in the contemporary era. BJU Int. 2017;119(5):676–83.
8. Weinreb JC, Barentsz JO, Choyke PL, et al. Eur Urol. 2015;69(1):16–40. PI-RADS Prostate Imaging - Reporting and Data System: 2015, Version 2[J].
9. Turkbey B, Rosenkrantz AB, Haider MA, et al. Eur Urol. 2019;76(3):340–51. Prostate Imaging Reporting and Data System Version 2.1: 2019 Update of Prostate Imaging Reporting and Data System Version 2.
10. Brembilla G, Dell'Oglio P. Stabile A, Preoperative multiparametric MRI of the prostate for the prediction of lymph node metastases in prostate cancer patients treated with extended pelvic lymph node dissection[J]. European Radiology.2017.
11. Hou Y, Bao ML, Wu CJ, Zhang J, Zhang YD, Shi HB, et al. A machine learning-assisted decision-support model to better identify patients with prostate cancer requiring an extended pelvic lymph node dissection. BJU Int. 2019;124(6):972–83.
12. Gandaglia G, Martini A, Ploussard G, et al. External validation of the 2019 Briganti nomogram for the identification of prostate cancer patients who should be considered for an extended pelvic lymph node dissection[J]. Eur Urol Open Sci. 2020;19:e1651–2.
13. Ying HA, Jie BC, Yang SD, et al. Integration of clinicopathologic identification and deep transferrable image feature representation improves predictions of lymph node metastasis in prostate cancer[J]. EBioMedicine. 2021;68(3):103395.
14. Créhange G, Chen CP, Hsu C, et al. Management of prostate cancer patients with lymph node involvement: a rapidly evolving paradigm[J]. Cancer Treat Rev. 2012;38(8):956–67.
15. Thoeny HC, Froehlich JM, Triantafyllou M, et al. Metastases in normal-sized pelvic lymph nodes: detection with diffusion weighted MR imaging. Radiology. 2014;273(1):125–35.
16. Muteganya R, Goldman S, Aoun F et al. Current imaging techniques for Lymph Node staging in prostate Cancer: a Review[J]. Front Surg. 2018;5.
17. Hövels AM, Heesakkers RAM, Adang EM, Jager GJ, Strum S, Hoogeveen YL, et al. The diagnostic accuracy of CT and MRI in the staging of pelvic lymph nodes in patients with prostate cancer: a meta-analysis. Clin Radiol. 2008;63:387–95.
18. von Below C, Daouacher G, Wassberg C, Grzegorek R, Gestblom C, Sörensen J, et al. Validation of 3 T MRI including diffusion-weighted imaging for nodal staging of newly diagnosed intermediate-and high-risk prostate cancer. Clin Radiol. 2016;71:328–34.
19. H?Vels AM, Heesakkers R, Adang EM, et al. The diagnostic accuracy of CT and MRI in the staging of pelvic lymph nodes in patients with prostate cancer: a meta-analysis.[J]. Clin Radiol. 2008;63(4):387–95.
20. Biondetti PR, Lee JKL, Ling D, et al. Clinical stage B prostate carcinoma staging with MR imaging. Radiology. 1987;162:325–9.
21. Hricak H, Dooms GC, Jeffrey RB, et al. Prostatic carcinoma:staging by clinical assessment, CT, and MR imaging. Radiology. 1987;162:331–6.
22. Morgan CL, Calkins RF, Cavalcanti EJ. Computed tomography in the evaluation, staging and therapy of carcinoma of the bladder and prostate. Radiology. 1981;140:751e61.
23. Flanigan RC, Mohler JL, King CT, et al. Preoperative lymph node evaluation in prostatic cancer patients who are surgical candidates: the role of lymphangiography and computerized tomography scanning with directed fifine needle aspiration. J Urol. 1985;134:84e7.

24. Alabousi M, Sala Me HJ, Gusenbauer K et al. Biparametric vs multiparametric prostate magnetic resonance imaging for the detection of prostate cancer in treatment-nave patients: a diagnostic test accuracy systematic review and meta-analysis[J]. BJU International.2019;124(2).

25. Peerlings J, Woodruff HC, Winfield JM et al. Stability of radiomics features in apparent diffusion coefficient maps from a multi-centre test-retest trial[J]. Sci Rep.2019; 9(1).

26. Epstein JI, Allsbrook WC Jr., Amin MB, E LL. The 2005 international society of urological pathology (ISUP) consensus conference on gleason grading of prostatic carcinoma. Am J Surg Pathol. 2005;29(9):1228–42.

27. Epstein JI, Egevad L, Amin MB, Delahunt B, Srigley JR, Humphrey PA. The 2014 international society of urological pathology (ISUP) Consensus conference on gleason grading of prostatic carcinoma: definition of grading patterns and proposal for a new grading system. J Surg Pathol. 2016;40(2):244–52.

28. Sanda MG, Cadeddu JA, Kirkby E, et al. Clinically localized prostate Cancer: AUA/ASTRO/SUO Guideline. Part I: Risk Stratification, Shared decision making, and Care Options[J]. J Urol. 2018;199(3):683–90.

29. Zhou Z, Qian X, Hu J, et al. An artificial intelligence-assisted diagnosis modeling software (AIMS) platform based on medical images and machine learning: a development and validation study[J]. Quant Imaging Med Surg. 2023;13(11):7504.

30. Kocak B, Baessler B, Bakas S, et al. CheckList for EvaluAtion of Radiomics research (CLEAR): a step-by-step reporting guideline for authors and reviewers endorsed by ESR and EuSoMII. Insights Imaging. 2023;14(1):75.

31. Kocak B, Akinci D'Antonoli T, Mercaldo N, et al. METhodological RadiomICs score (METRICS): a quality scoring tool for radiomics research endorsed by EuSoMII. Insights Imaging. 2024;15(1):8.

32. Chawla NV, Bowyer KW, O.Hall L, Kegelmeyer WP. SMOTE: synthetic minority over-sampling technique. J Artif Intell Res. 2002; 321–57.

33. Segal E, Sirlin CB, Ooi C, et al. Decoding global gene expression programs in liver cancer by noninvasive imaging[J]. Nat Biotechnol Jun. 2007;25(6):675–80.

34. Radiomics. Extracting more information from medical images using advanced feature analysis. Eur J Cancer. 2012;48(4):441–6.

35. Zheng H, Miao Q, Liu Y, et al. Multiparametric MRI-based radiomics model to predict pelvic lymph node invasion for patients with prostate cancer. Eur Radiol. 2022;32(8):5688–99.

36. Wang T, Gao T, Yang J, Yan X, Wang Y, Zhou X, et al. Preoperative prediction of pelvic lymph nodes metastasis in early-stage cervical cancer using radiomics nomogram developed based on T2-weighted MRI and diffusion-weighted imaging. Eur J Radiol. 2019;114:128–35.

37. Huang YQ, Liang CH, He L, Tian J, Liang CS, Chen X, et al. Development and validation of a radiomics nomogram for preoperative prediction of lymph node metastasis in colorectal cancer. J clin Oncol off J Am Soc Clin Oncol. 2016;34(18):2157–64.

38. Fortuin AS, Meijer H, Thompson LC, et al. Ferumoxtran-10 ultrasmall superparamagnetic iron oxide-enhanced diffusion-weighted imaging magnetic resonance imaging for detection of metastases in normal-sized lymph nodes in patients with bladder and prostate cancer: do we enter the era after extended pelvic lymph node dissection?[J]. Eur Urol. 2013;64(6):961–3.

39. Fortuin AS, Deserno WM, Meijer HJ, et al. Value of PET/CT and MR Lymphography in treatment of prostate cancer patients with lymph node metastases. Int J Radiat Oncol Biol Phys. 2012;84(3):712–8.

40. Triantafyllou M, Studer UE, Birkh?User FD, et al. Ultrasmall superparamagnetic particles of iron oxide allow for the detection of metastases in normal sized pelvic lymph nodes of patients with bladder and/or prostate cancer[J]. Eur J Cancer. 2013;49(3):616–24.

41. Birkh?User FD, Studer UE, Froehlich JM, et al. Combined ultrasmall superparamagnetic particles of iron oxide-enhanced and diffusion-weighted magnetic resonance imaging facilitates detection of metastases in normal-sized pelvic lymph nodes of patients with bladder and prostate cancer.[J]. Eur Urol. 2013;64(6):953–60.

42. Nketiah G, Elschot M, Kim E, et al. T2-weighted MRI-derived textural features reflect prostate cancer aggressiveness: preliminary results[J]. Eur Radiol. 2016;27(7):3050–9.

43. Wibmer A, et al. Haralick texture analysis of prostate MRI: utility for differentiating non-cancerous prostate from prostate cancer and differentiating prostate cancers with different Gleason scores. Eur Radiol. 2015;25:2840–50.

44. Nketiah GA, Elschot M, Scheenen TW, et al. Utility of T2-weighted MRI texture analysis in assessment of peripheral zone prostate cancer aggressiveness: a single-arm, multicenter study. Sci Rep. 2021;11:2085.

45. Li M, Zhang J, Dan Y et al. A clinical-radiomics nomogram for the preoperative prediction of lymph node metastasis in colorectal cancer[J]. J Translational Med.2020;18(1).

Publisher's Note